Materials Views
www.MaterialsViews.com

ADVANCED ENERGY MATERIALS
www.advmat.de

High-Efficiency Solar Cell with Earth-Abundant Liquid-Processed Absorber

By *Teodor K. Todorov, Kathleen B. Reuter,* and *David B. Mitzi**

Chalcogenide-based solar cells provide a critical pathway to cost parity between photovoltaic (PV) and conventional energy sources. Currently, only $Cu(In,Ga)(S,Se)_2$ (CIGS) and CdTe technologies have reached commercial module production with stable power conversion efficiencies of over 9 percent.[1,2] Despite the promise of these technologies, restrictions on heavy metal usage for Cd and limitations in supply for In and Te are projected to restrict the production capacity of the existing chalcogen-based technologies to <100 GWp per year, a small fraction of our growing energy needs, which are expected to double to 27 TW by 2050.[3–5] Earth-abundant copper-zinc-tin-chalcogenide kesterites, Cu_2ZnSnS_4 and $Cu_2ZnSnSe_4$, have been examined as potential alternatives for the two leading technologies,[6–9] reaching promising but not yet marketable efficiencies of 6.7% and 3.2%, respectively, by multilayer vacuum deposition.[7,8] Here we show a non-vacuum, slurry-based coating method that combines advantages of both solution processing[10–13] and particle-based deposition,[14–17] enabling fabrication of $Cu_2ZnSn(Se,S)_4$ devices with over 9.6% efficiency—a factor of five performance improvement relative to previous attempts to use high-throughput ink-based approaches[16–18] and >40% higher than previous record devices prepared using vacuum-based methods.[7]

To address the issue of cost, non-vacuum ''ink''-based approaches—both from solutions and suspensions—are being developed for chalcogenide-based absorber layer deposition to replace potentially more expensive vacuum-based techniques.[11–19] True solutions allow intermixing of the constituents at a molecular level and the formation of smooth homogeneous films, as demonstrated with spin-coated CIGS absorber layers from hydrazine (N_2H_4) solutions.[11–13] The chemically reducing character of hydrazine stabilizes solutions of anions with direct metal-chalcogen bonding for select elements (e.g. Cu, In, Ga, Sn), without the necessity to introduce typical impurities (e.g., C, O, Cl).[10,11,20] Suspension approaches employ solid particles designed to be deposited on a substrate and reacted or fused with each other, to form a desired crystalline phase and grain structure.[14,15] Normally insoluble components can be deposited by this approach using typical liquid-based deposition (e.g., printing, spin coating, slit casting, spraying).

Although high-quality large-grained absorber layers can be formed for selected systems using either solution- or particle-based deposition,[11–15,19] numerous challenges confront each approach for more general deposition needs. Solution processing is limited by the solubility of many materials of interest (e.g., $ZnSe_{1-x}S_x$ in hydrazine solvents—relevant for the deposition of Cu_2ZnSnS_4 or $Cu_2ZnSnSe_4$). In addition, volume contraction upon drying of solution-deposited layers creates stress in the film that may cause crack formation in thicker films. In suspension approaches, a common difficulty is achieving single-phase crystallization among the solid particles. Particle-based approaches (as well as some solution methods) typically require the addition of organic agents to improve wetting and particle dispersion, and to avoid film cracks and delamination. Most of these non-volatile organic additives introduce carbon contamination in the final layer. Because of these challenges, vacuum-based techniques have historically shown superior performance to liquid coating. In the case of the earth-abundant $Cu_2ZnSn(S,Se)_4$ materials, ink-based approaches have to date yielded at most <1.6% efficiency devices.[16–18,21]

Here we demonstrate an hybrid solution-particle approach, using the earth-abundant $Cu_2ZnSn(S,Se)_4$ system as an example, which enables fabrication of PV devices with over 9.6% power conversion efficiency. The slurry (or ink) employed for deposition comprises a Cu–Sn chalcogenide (S or S–Se) solution in hydrazine (see *Experimental* section),[10–13] with the in situ formation of readily dispersible particle-based Zn-chalcogenide precursors, $ZnSe(N_2H_4)$ (Figure 1a,d) or $ZnS(N_2H_4)$ (Figure 1b). Thermogravimetric analysis (TGA) of the isolated selenide particle precursor shows decomposition at approximately 200 °C, with mass loss of about 20%, close to the theoretical value expected upon transition to pure ZnSe (Figure 1c,d). Deposition using this hybrid slurry successfully combines the advantages of solution and suspension deposition routes by use of solutions containing solid particles, wherein both components (i.e., solution and particle) contain metal and chalcogen elements that integrate into the final film. Using the hybrid slurry method (i) solubility limitations are resolved, as virtually any materials system can be constituted by a combination of solid and dissolved components; (ii) the dissolved components can be engineered as an efficient binding media for the particles, eliminating the need of separate organic binders; (iii) solid particles act as stress-relief and crack-deflection centers allowing the deposition of thicker layers than pure solution processes; and (iv) the intimate contact between the two phases allows rapid reaction and homogeneous phase formation.

Complete conversion of all constituents of the spin-coated hybrid precursor films into a single-phase, highly crystalline $Cu_2ZnSn(S,Se)_4$ is achieved by annealing at 540 °C on a hot plate. Three main types of samples were targeted – high selenium content (A), intermediate sulfoselenide (B) and pure sulfide (C) –

[*] Dr. D. B. Mitzi, Dr. T. K. Todorov, Dr. K. B. Reuter
IBM T. J. Watson Research Center, P.O. Box 218, Yorktown Heights, NY 10598, USA
E-mail: dmitzi@us.ibm.com

DOI: 10.1002/adma.200904155

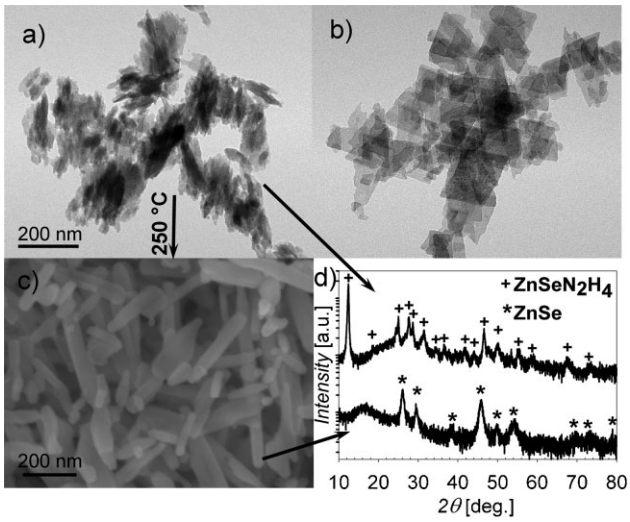

Figure 1. Particle-based components of the hybrid precursors used in the present work: a) $ZnSe(N_2H_4)$ and b) $ZnS(N_2H_4)$ particles isolated from the $Cu_2ZnSn(S,Se)_4$ precursor slurries by filtration; c) ZnSe product of the thermal decomposition of the pure $ZnSe(N_2H_4)$ particle precursor at 250 °C under inert atmosphere. The resulting nanorod ZnSe material was found to remain virtually unchanged (when annealed in isolated form) up to the maximum working temperature of 540 °C. d) X-ray diffraction patterns of the particle component of the selenide precursor before and after the 540 °C anneal.

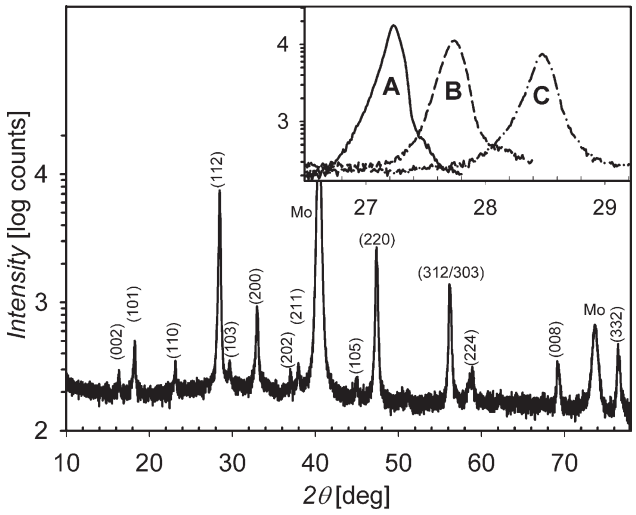

Figure 2. X-ray diffraction pattern of sulfide sample C, Cu_2ZnSnS_4, identified as kesterite, JCPDS 26-0575. Peaks arising from the Mo underlayer are noted. Inset: (112)-peak shift with progressively increased sulfur content in samples A, B and C (same axis labeling as for the main figure). The fitted tetragonal lattice constants (using full diffraction profile) for each of the samples are—Sample A: $a = 5.668(2)$ Å, $c = 11.349(5)$ Å; Sample B: $a = 5.567(1)$ Å, $c = 11.168(2)$ Å; Sample C: $a = 5.432(1)$ Å, $c = 10.840(3)$ Å.

as controlled using solution stoichiometry and heat treatment conditions (see *Experimental*). In each case, metal stoichiometry was selected to yield Cu-poor and Zn-rich compositions (approximately $Cu/Zn + Sn = 0.8$ and $Zn/Sn = 1.2$) similar to those described for previous record devices.[7] Examination of X-ray diffraction (XRD) data for each film (Figure 2) demonstrates a single-phase kesterite film with unit cell volume increasing from $V = 319.9$ Å^3 for sample C to 346.1 Å^3 and 364.6 Å^3 for samples B and A, respectively, as the larger Se replaces the smaller S atom. No unidentified peaks were observed in the XRD data, demonstrating well-crystallized and single phase films. The measured lattice constants of films A and C are in good agreement with literature values for $Cu_2ZnSnSe_4$ ($V = 366.8$ Å^3)[8] and Cu_2ZnSnS_4 ($V = 319.5$ Å^3; data from JCPDS 26-0575), respectively.

High-performance photovoltaic devices were fabricated from Se-rich (A) and sulfoselenide (B) layers, deposited as described above. A cross-section scanning electron microscopy (SEM) image of a device including an A-type film (Figure 3a) shows a $Cu_2ZnSn(S,Se)_4$ layer comprising large grains (1–2.5 μm), but also some isolated voids. Further processing refinement will likely lead to improvement in device performance as void volume is reduced. A cross-section transmission electron microscopy (TEM) comparison between sample types A and B (Figure 3b,c), demonstrates that varying the Se:S ratio has little impact on the grain size. Compositional profiling demonstrates homogeneous metal distribution within the absorber and confirms the higher S/(S + Se) ratio in Sample B (~0.4) in comparison with Sample A (~0.08) (Figure 3d). Note that these relatively thick (>2.5 μm) films can be achieved with only 5 deposition cycles (Figure 3a). Preliminary experiments have demonstrated that single-layer thickness can exceed 1 micrometer using the hybrid particle solution approach without substantial film cracking or peeling, perhaps because of the improved stress relief character provided to the precursor film by the solid Zn(S,Se) particles embedded in the metal chalcogenide matrix. This factor is expected to ultimately enable complete PV absorber fabrication using one or two coating cycles.

Device electrical characterization was certified by the National Renewable Energy Laboratory (NREL) PV Cell Performance Laboratory (Figure 4a), in agreement with measurements performed within our lab. Remarkably high photocurrents (36.4 mA cm^{-2}) are observed in the Se-rich device A, while higher voltages (516 mV) and also best total area device power conversion efficiency (9.66%) were measured in mixed sulfoselenide device B. The higher sulfur content of sample B evidently causes an optical band gap increase from 1.0 eV (A) to 1.2 eV (B), as calculated from the quantum efficiency data (Figure 4b). Despite the early stage of optimization for this process, the demonstrated device efficiencies are >40% higher than the previous record for $Cu_2ZnSn(S,Se)_4$ deposited by any means,[7] demonstrating that solution-based techniques can effectively compete with vacuum-based approaches not only with respect to cost, but also in achieving highest possible electrical performance. Apart from the "champion device" examples shown in Figure 4, more than 20 solar cells with efficiencies above 8% have been fabricated under different conditions, demonstrating a substantial degree of robustness to this approach even at this early stage of development.

Particular significance is given to the fact that record PV device performance has been achieved in this case with simple liquid-based processing, which can be adapted to numerous ultrahigh throughput printing (e.g., flexographic, screen, ink-jet) and coating (e.g., spin, spray, curtain, slit) techniques, some of

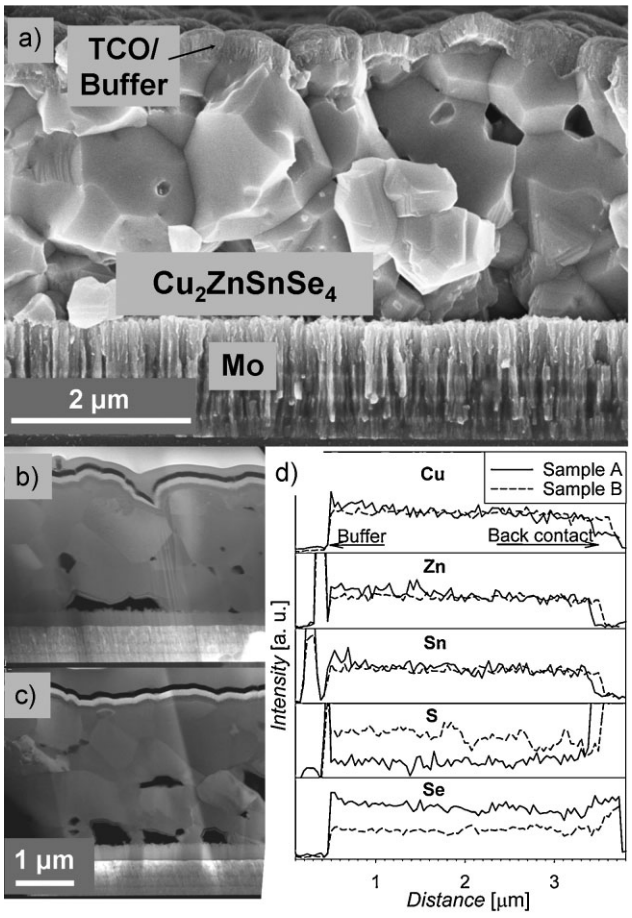

Figure 3. a) Cross section SEM image of a type A device, with structure consisting of glass substrate/Mo back contact (800 nm)/spin-coated $Cu_2ZnSn(S,Se)_4$/CdS (60 nm)/ZnO (80 nm)/ITO (130 nm). Note that between the Mo and $Cu_2ZnSn(S,Se)_4$ layer there is a relatively thick (~300 nm) $MoSe_2$ interfacial layer, as is more evident in the TEM cross sections. b,c) TEM cross sections of type A and B devices, respectively. d) Transmission EDX compositional profiling showing uniform metal composition and higher S content in sample B.

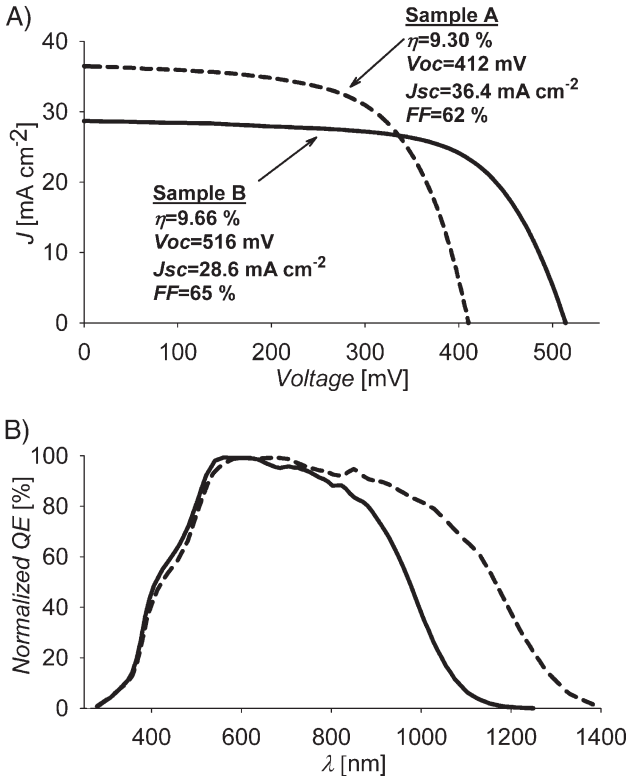

Figure 4. *J–V* characteristics under standard ASTM G173 global spectrum (certified by NREL PV Cell Performance Laboratory) of devices with low (A) and intermediate (B) sulfur content, showing higher V_{oc} and efficiency in the second case. The efficiencies are calculated using total area of the device (including Ni/Al grid-covered area).

which are capable of handling substrate speeds exceeding 1000 m min^{-1} in a roll-to-roll configuration.[22] The described hybrid liquid-particle based approach therefore expands the possibilities for development of scalable and low-cost manufacturing techniques for Cu–Zn–Sn–Se–S absorbers, as well as potentially other multinary chalcogenide semiconductors known to present processing challenges due to their compositional complexity. Bypassing limitations of pure solution-based approaches, such as insoluble components, and gaining advantages, including additive-free layer formation and targeted nucleation, enables high crystalline quality and chemical purity of the obtained materials and films. Furthermore, the remarkable flexibility to readily tailor the stoichiometry of resulting films, simply by controlled addition of starting materials in either of the two slurry components, facilitates the development and optimization of materials beyond PV absorbers, such as chalcogenide-based semiconducting materials for optical or electronic applications (e.g., phase change and electrolytic memory, transistors, non-linear optical materials).[10,23–25]

Experimental

Film Preparation: Hydrazine solution preparation and spin coating were performed in a nitrogen-filled glove box, following procedures described elsewhere[10–13]. *Caution: hydrazine must be handled using appropriate protective equipment to prevent physical contact with either vapor or liquid*. For the selenosulfide films A and B, individual Cu_2S–S (1.2 M) and SnSe–Se (0.57 M) hydrazine solutions were first prepared. Readily dispersible $ZnSe(N_2H_4)$ particles were formed in situ by the stoichiometric addition of elemental zinc powder directly to the tin solution. For both the Cu and Sn/Zn solutions, additional chalcogen was added to facilitate dissolution of the metal chalcogenide[10–13] and enable full reaction with the Zn powder. The Sn/Zn and Cu solutions were mixed, targeting final composition $Cu/(Zn+Sn)=0.8$ and $Zn/Sn=1.22$, with a nominal kesterite $Cu_{2-x}Zn_{1+y}Sn(S,Se)_4$ concentration in the resulting solution of approximately 0.4 M. An analogous solution was prepared for the pure sulfide film C, but with all of the components (Cu_2S, SnS, S and Zn powder) mixed in one batch, leading to in situ formation of $ZnS(N_2H_4)$. For each film, five successive layers were spin coated at 800 rpm and annealed on a ceramic hot plate at 540 °C. Sulfur content adjustment for sample B was achieved by use of elemental sulfur vapor during final heat treatment (no extra elemental chalcogen was added during heat treatment of samples A or C).

$ZnS(N_2H_4)$ and/or $ZnSe(N_2H_4)$ particles were isolated for XRD, TEM and TGA analysis by filtration from the deposition solution, followed by rinsing with hydrazine.

Device Fabrication: Solar cells were formed on Mo-coated glass substrates, using the above described $Cu_2ZnSn(S,Se)_4$ films and a standard CIGS device structure (see Figure 3 caption; targeted device area is 0.45 cm^2)[11–13]. A Ni-Al collection grid and 110-nm-thick MgF_2 antireflection coating were deposited on top of the device by electron-beam evaporation.

Characterization: Powder X-ray data were collected using a Siemens D5000 diffractometer with Cu Kα radiation. Pawley refinements[26] of structural parameters were performed from the full diffraction profile (Figure 2) using the Bruker Topas(P) software package (version 2.1) and initial cell constants from the PDF card for Cu_2ZnSnS_4 (26-0575). SEM was conducted on the $Cu_2ZnSn(S,Se)_4$ films, which were cleaved prior to the SEM analyses and coated with a thin Pd–Au film to prevent charging effects. Samples for TEM/STEM (scanning transmission electron microscopy) analysis were prepared using the FEI Helios 400S DB–FIB. TEM images were taken using a JEOL 3000F TEM operated at 300 kV. Compositional profiles were acquired by STEM/EDX (energy dispersive X-ray spectroscopy). The incident electron probe comprised 300keV electrons in an incident probe of 0.7 nm full-width at half-maximum (FWHM).

Acknowledgements

The authors thank A. Prabhakar, J. Chey, R. Ferlita and W. Liu for their help in substrate preparation and device fabrication; and K. Emery and P. Ciszek, of the NREL PV Cell Performance Laboratory, for the PV device certification shown in Figure 4.

Received: December 4, 2009
Published online: February 8, 2010

[1] M. A. Green, K. Emery, Y. Hishikawa, W. Warta, *Prog. Photovolt.: Res. Appl.* **2009**, *17*, 85.
[2] D. Butler, *Nature* **2008**, *454*, 558.
[3] N. S. Lewis, D. G. Nocera, *Proc. Natl. Acad. Sci. USA* **2006**, *103*, 15729.
[4] B. A. Andersson, *Prog. Photovolt.: Res. Appl.* **2000**, *8*, 61.
[5] C. Wadia, A. P. Alivisatos, D. M. Kammen, *Environ. Sci. Technol.* **2009**, *43*, 2072.
[6] K. Ito, T. Nakazawa, *Jpn. J. Appl. Phys.* **1988**, *27*, 2094.
[7] H. Katagiri, K. Jimbo, W. S. Maw, K. Oishi, M. Yamazaki, H. Araki, A. Takeuchi, *Thin Solid Films* **2009**, *517*, 2455.
[8] G. Zoppi, I. Forbes, R. W. Miles, P. J. Dale, J. J. Scragg, L. M. Peter, *Prog. Photovolt.: Res. Appl.* **2009**, *17*, 315.
[9] R. Schurr, A. Hölzing, S. Jost, R. Hock, T. Voβ, J. Schulze, A. Kirbs, A. Ennaoui, M. Lux-Steiner, A. Weber, I. Kötschau, H.-W. Schock, *Thin Solid Films* **2009**, *517*, 2465.
[10] D. B. Mitzi, L. L. Kosbar, C. E. Murray, M. Copel, A. Afzali, *Nature* **2004**, *428*, 299.
[11] D. B. Mitzi, M. Yuan, W. Liu, A. J. Kellock, S. J. Chey, V. Deline, A. G. Schrott, *Adv. Mater.* **2008**, *20*, 3657.
[12] D. B. Mitzi, *Adv. Mater.* **2009**, *21*, 3141.
[13] D. B. Mitzi, M. Yuan, W. Liu, A. J. Kellock, S. J. Chey, L. Gignac, A. G. Schrott, *Thin Solid Films* **2009**, *517*, 2158.
[14] V. K. Kapur, A. Bansal, P. Le, O. I. Asensio, *Thin Solid Films* **2003**, *431–432*, 53.
[15] J. K. J. van Duren, C. Leidholm, A. Pudov, M. R. Robinson, Y. Roussillon, *Mater. Res. Soc. Symp. Proc.* **2007**, *1012*, Y05–03.
[16] C. Steinhagen, M. G. Panthani, V. Akhavan, B. Goodfellow, B. Koo, B. A. Korgel, *J. Am. Chem. Soc.* **2009**, *131*, 12554.
[17] Q. Guo, H. W. Hillhouse, R. Agrawal, *J. Am. Chem. Soc.* **2009**, *131*, 11672.
[18] N. Moritake, Y. Fukui, M. Oonuki, K. Tanaka, H. Uchiki, *Phys. Status Solidi C* **2009**, *6*, 1233.
[19] T. Todorov, D. B. Mitzi, *Eur. J. Inorg. Chem.* **2010**, *2010*, 17.
[20] M. Yuan, D. B. Mitzi, *Dalton Trans.* **2009**, 6078.
[21] T. Todorov, M. Kita, J. Carda, P. Escribano, *Thin Solid Films* **2009**, *517*, 2541.
[22] F. C. Krebs, *Solar Energy Mater. Solar Cells*, **2009**, *93*, 394.
[23] T. Ohta, *J. Optoelectron. Adv. Mater.* **2001**, *3*, 609.
[24] M. Kozicki, M. Mitkova, *J. Non-Cryst. Solids* **2006**, *352*, 567.
[25] A. Zakery, S. R. Elliott, *J. Non-Cryst. Solids* **2003**, *330*, 1.
[26] G. S. Pawley, *J. Appl. Crystallogr.* **1981**, *14*, 357.